Particle velocity in geoacoustics: A performance study based on ensemble adjoint inversion

Jean-Pierre Hermand[1], Mohamed Berrada[1,2,3], Mark Asch[3]

1Université libre de Bruxelles, Laboratoire d' Hydroacoustique Environnementale, av. Franklin D. Roosevelt 50 - CP 194/05, B-1050 Bruxelles, Belgium, jhermand@ulb.ac.be
2 Université Pierre et Marie Curie, Laboratoire d'Océanographie et du Climat - Exp´erimentation et Approches Num´eriques (CNRS UMR 7159), Tour 45-55, 5éme étage 4, place Jussieu, 75005 Paris, France, mohamed.berrada@upmc.fr
3Université de Picardie Jules Verne, Laboratoire Amiénois de Mathématique Fondamentale et Appliquée (CNRS UMR 6140), 33 Rue Saint Leu, 80039Amiens, France, mark.asch@u-picardie.fr

Particle velocity in geoacoustics: A performance study based on ensemble adjoint inversion

Jean-Pierre Hermand[1], Mohamed Berrada[1,2,3], Mark Asch[3]

[1]Université libre de Bruxelles, Laboratoire d' Hydroacoustique Environnementale, av. Franklin D. Roosevelt 50 - CP 194/05, B-1050 Bruxelles, Belgium, **jhermand@ulb.ac.be**

[2] Université Pierre et Marie Curie, Laboratoire d'Océanographie et du Climat - Expérimentation et Approches Numériques (CNRS UMR 7159), Tour 45-55, 5-ème étage 4, place Jussieu, 75005 Paris, France, **mohamed.berrada@upmc.fr**

[3]Université de Picardie Jules Verne, Laboratoire Amiénois de Mathématique Fondamentale et Appliquée (CNRS UMR 6140), 33 Rue Saint Leu, 80039 Amiens, France, **mark.asch@u-picardie.fr**

In the last decade or so, methods for the physical characterization of marine sediment have been developed that use waterborne acoustic (scalar) pressure field measured on a hydrophone array and a global optimization scheme based on some form of matched field processing (MFP). In this paper, the benefit of additional information of co-located (vector) particle velocity measurement is investigated. An actual measurement setup of MREA/BP07 experiment is simulated to assess the relative sensitivity of pressure and vertical particle velocity fields to the geoacoustic parameters of a layered bottom and the respective robustness to uncertainty. An ensemble adjoint approach is proposed wherein the inversion process itself is directly and optimally controlled by the physics of acoustic propagation, in contrast to metaheuristic global optimization. In this first comparative study, the inversion is carried out jointly across multiple frequencies by minimizing a Bartlett cost function for the pressure and vertical particle velocity components taken separately. A multidimensional Monte Carlo technique is applied to the initial conditions and measurement noise realizations. The ensemble results suggest that vertical particle velocity can enhance the estimation of density and attenuation parameters of the layered bottom.

1 Introduction

Acoustic vector sensor measures the acoustic pressure and all three orthogonal components of the acoustic particle velocity at a point of space. Vector sensor arrays (VSA) have drawn much attention in recent years because of a number of advantages over (scalar) hydrophone arrays: they allow for a full azimuth and elevation estimation in a vertical line configuration, do not suffer from the left/right ambiguity that occurs in a tow configuration and can be used in an effective, sparse and compact configuration for, e.g., low-frequency beamforming. To date few results have been published on the use of VSA's for geoacoustic characterization [1–7]. Recent experimental results showed that a sparse and compact, vertical array of traditional hydrophones in combination with model-based matched filter processing can be very effective in inverting for the geoacoustic parameters of a soft layered bottom [8,9]. In this paper, an actual measurement situation is simulated by replacing the array pressure sensors (hydrophones) with vector sensors. The pressure-based experimental results serve as a baseline for assessing the sensitivity of the vertical component of particle velocity to environmental parameters, and in particular bottom density and acoustic attenuation parameters which are difficult to obtain. An ensemble adjoint approach is proposed that is particularly effective for the comparative study because the inversion process itself is directly and optimally controlled by the physics of acoustic propagation. Sec. 2–4 describes the adjoint wide-angle PE modeling and its extension to particle velocity, the cost function and its minimization. Sec. 5 presents the reference environment and measurement setup. Sec. 6 presents ensemble inversion results for selected examples. Sec. 7 concludes the paper.

2 A wide-angle PE for particle velocity

Let G be an ocean-acoustic propagation model predicting the acoustic state $\mathbf{d}$ and $\mathbf{m}$ a vector of environmental parameters. The vector $\mathbf{m}$ is the input of G and $\mathbf{d}$ its output

$$\mathbf{d} = G(\mathbf{m}). \tag{1}$$

The numerical (direct) model G is based here on the wide-angle parabolic equation (WAPE) due to Claerbout [10] associated with a non-local boudary condition (NLBC) due to Yevick and Thomson [11]. For a stratified medium with varying density $\rho(z)$, sound speed $c(z)$ and absorption loss $\lambda(z)$ the analytical WAPE model can be obtained as [12]

$$\left\{\begin{array}{l} 2ik_0\left(1+\frac{1}{4}(\mathcal{N}^2-1)\right)\frac{\partial\psi}{\partial r}+\rho\frac{\partial}{\partial z}\rho^{-1}\frac{\partial\psi}{\partial z} \\ \qquad +k_0^2(\mathcal{N}^2-1)\psi+\frac{i}{2k_0}\rho\frac{\partial}{\partial z}\rho^{-1}\frac{\partial^2\psi}{\partial z\partial r}=0, \\ \psi(0,z)=S_f(z), \\ \psi(r,0)=0, \\ \text{and the NLBC} \\ \quad \left[\frac{\partial}{\partial z}-i\beta\right]\psi(r+\Delta r,z_b)= \\ \qquad i\beta\sum_{j=1}^{K+1}\mathbf{g}_{1,j}\psi\left[(K+1-j)\Delta r,z_b\right], \end{array}\right. \tag{2}$$

where $k_0 = 2\pi f/c_0$ is a reference wave number, c_0 is a reference sound speed, $\mathcal{N}(z) = n(z)[1+i\alpha(z)]$, $n(z) =$

$c_0/c(z)$ is the refraction index, $S_f(z)$ is an analytical source term and β is defined as

$$\beta = \frac{\rho_w}{\rho_b} k_0 \sqrt{\frac{(\mathcal{N}_b^2 - 1)(1 + \frac{1}{4}\mu^2) + \mu^2}{1 + \frac{1}{4}\mu^2}}, \tag{3}$$

where $\mu^2 = 4i/k_0\Delta r$, and the subscripts w and b denote the water column and bottom, respectively. For further details on the NLBC derivation, including algebraic expressions for the coefficients $\mathbf{g}_{1,j}$, see [13]. The field $\psi(r, z)$ is related to the acoustic pressure $p(r, z)$ by

$$p(r, z) = \frac{\psi(r, z) \exp(ik_0 r)}{\sqrt{k_0 r}}. \tag{4}$$

Acoustic particle velocity $\mathbf{v}$ is defined as the gradient of the acoustic pressure

$$\mathbf{v} = -\frac{i}{\omega\rho_0} \nabla p, \tag{5}$$

which, in cylindrical coordinates and by neglecting the azimuthal component, can be written as

$$\mathbf{v}(r, z) = -\frac{i}{\omega\rho_0} \left[\frac{\partial p}{\partial r} \hat{\mathbf{r}} + \frac{\partial p}{\partial z} \hat{\mathbf{z}} \right]. \tag{6}$$

The output of the acoustic vector model G consists of three complex-valued components: the pressure defined by (4) and the two components of the particle velocity $\mathbf{v}$ defined by (6). Each component is measured and predicted at N range and depth positions giving rise to a vector $\mathbf{d}$ of $3N$ elements. One can rewrite (1) as

$$\mathbf{d} = \begin{pmatrix} p \\ v_r \\ v_z \end{pmatrix} = G(\mathbf{m}), \tag{7}$$

where p is the acoustic pressure and v_r and v_z are respectively the radial (horizontal) and vertical components of the particle velocity $\mathbf{v}$. In a 3-dimensional situation the acoustic state vector can be augmented by the azimuthal component.

The numerical implementation of the acoustic vector model G is obtained by a finite difference discretization of the above equations. In the following one denotes $\mathbf{d}_1 = G_1(\mathbf{m})$ the first component of $\mathbf{d}$ (i.e., p), and $\mathbf{d}_2 = G_2(\mathbf{m})$ and $\mathbf{d}_3 = G_3(\mathbf{m})$ its second and third components (i.e., v_r and v_z respectively).

3 Cost function and adjoint implementation

Let $\mathbf{y}_0$ be the observation vector of the acoustic state. $\mathbf{y}_0$ as $\mathbf{d}$ is a vector of $3N$ elements and is composed of three components $\mathbf{y}_{k,0}$ $(k = 1, 2, 3)$. Following [3] a cost function based on the Bartlett processor is thus defined for the kth component as

$$J_k(\mathbf{m}) = \mathrm{tr}\mathbf{R}_k - \frac{\mathbf{d}_k^\dagger \mathbf{R}_k \mathbf{d}_k}{\|\mathbf{d}_k\|^2}, \tag{8}$$

where $\dagger$ is the Hermitian transpose operator, tr is the trace operator, $\|\mathbf{d}_k\|^2 = \mathbf{d}_k^\dagger \mathbf{d}_k$, $\mathbf{R}_k = \mathbf{y}_{k,0}\mathbf{y}_{k,0}^\dagger / \|\mathbf{y}_{k,0}\|^2$ is the estimate of the cross-spectral density (or covariance) matrix of the observed data in "phone space", and $\mathrm{tr}\mathbf{R}_k = 1$. See [14, 15] for more detail about this cost function.

The minimization of J_k in (8) is done by a gradient descent method. The gradient of J_k with respect to $\mathbf{m}$ is given by

$$\nabla_{\mathbf{m}} J_k(\mathbf{m}) = \mathcal{G}_k^\dagger \nabla_{\mathbf{d}_k} J_k, \tag{9}$$

where $\mathcal{G}_k = \partial G_k / \partial \mathbf{m}$ is the so-called tangent linear model of the direct model G_k and $\mathcal{G}_k^\dagger$ is the adjoint model. From (8) and (9), the gradient of J_k with respect to $\mathbf{d}_k$, $\nabla_{\mathbf{d}_k} J_k$, is given by

$$\nabla_{\mathbf{d}_k} J_k = -\frac{\mathbf{R}_k \mathbf{d}_k}{\|\mathbf{d}_k\|^2} + \frac{(\mathbf{d}_k^\dagger \mathbf{R}_k \mathbf{d}_k)\mathbf{d}_k}{\|\mathbf{d}_k\|^4}. \tag{10}$$

Therefore, the gradient of the cost function J_k with respect to $\mathbf{m}$ is obtained as

$$\nabla_{\mathbf{m}} J_k(\mathbf{m}) = \mathcal{G}_k^\dagger \left(-\frac{\mathbf{R}\mathbf{d}_k}{\|\mathbf{d}_k\|^2} + \frac{(\mathbf{d}_k^\dagger \mathbf{R}\mathbf{d}_k)\mathbf{d}_k}{\|\mathbf{d}_k\|^4} \right). \tag{11}$$

It is well established that observations at multiple frequencies provide valuable additional information for environmental inversion, see e.g., [14]. The cost function and its gradient are then extended to multiple frequencies by summing the contribution of each frequency. For multiple frequencies f_i $(i = 1, \ldots, L)$ the cost function (8) becomes

$$\mathcal{J}_k(\mathbf{m}) = \sum_{i=1}^{L} J_k^i(\mathbf{m}) = \sum_{i=1}^{L} \mathrm{tr}\mathbf{R}_k^i - \frac{\mathbf{d}_k^{i\dagger} \mathbf{R}_k^i \mathbf{d}_k^i}{\|\mathbf{d}_k^i\|^2}. \tag{12}$$

The gradient of (12) is thus given by

$$\nabla_{\mathbf{m}} \mathcal{J}_k(\mathbf{m}) = \sum_{i=1}^{L} \nabla_{\mathbf{m}} J_k^i(\mathbf{m}). \tag{13}$$

The next step to develop the inversion scheme is the numerical implementation of the adjoint model for pressure and particle velocity $\mathcal{G}_k^\dagger$ $(k = 1, 2, 3)$. In previous work a modular graph approach [13] has been used through the semi-automatic adjoint generator YAO [16] to implement the adjoint model for pressure, and then for particle velocity which is calculated locally from the pressure field. For a detailed discussion about the adjoint implementation see [3, 13, 17].

4 Minimization process

For the minimization process, the routine M2QN1 of Ref. [18] is used, which is designed to minimize functions depending on a small or medium number of variables m_i subject to bound constraints $(a_i \leq m_i \leq b_i)$ and implements a quasi-Newton method with the BFGS [19] technique for the estimation of the Hessian at the next iteration. Other parameters that the bounds a_i and b_i are to be specified to the

minimizer M2QN1. These parameters are the stopping criterion on the Kuhn-Tucker conditions [20] (denoted epsg), and the resolution argument dmmin_i in the coordinate m_i of the control vector $\mathbf{m}$. The parameter dmmin_i also serves to determine the bound accuracy and to make a change of variable $\tilde{m}_i = m_i/\mathsf{dmmin}_i$, which has an influence on the stopping criterion. To avoid the choice of dmmin_i for each variable of the control vector the following normalization is proposed

$$m' = \frac{m - m_t}{\theta}, \tag{14}$$

where m' is the normalized parameter, m_t is the "true" value and θ is a coefficient.

5 Reference environment and measurement setup

In the spring of 2007, Maritime Rapid Environmental Assessment (MREA/BP07) experiments were carried out southeast of the Elba Island in the Mediterranean Sea [21]. In acoustic run #2 [8], schematized in Fig. 1, a broadband sound source was positioned in the lower part of the water column and a vertical ocean acoustic array (OAA) of four equispaced hydrophones was positioned in the upper part of the water column. The receiver drifted toward the source over ranges from about 13 to 7 times the water depth. For comparison purpose a range of 1161 m is chosen for which geoacoustic inversion results were presented in [8]. The

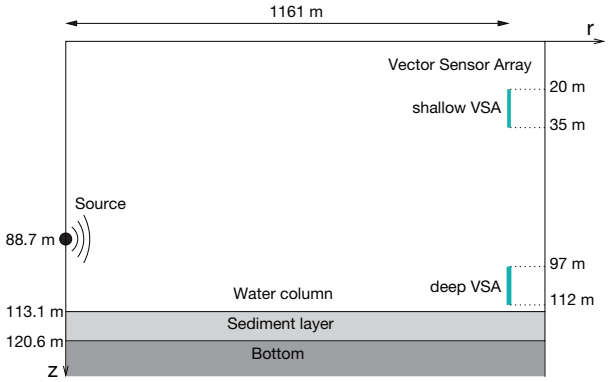

Figure 1: Geometry of source-receiver and environment for acoustic run #2 of MREA/BP07 experiment, April 23rd, 2007. A multifrequency source was positioned at $z_s = 88.7$-m depth. The range-average water depth is $z_l = 113.1$ m and the bottom halfspace depth is $z_b = 120.6$ m. The pressure (OAA) or vector sensor array (VSA) is at $r_{\max} = 1161$ m distance from the source. Depths of the shallow VSA elements: 20.1 m, 25.1 m, 30.1 m and 35.1 m. Depths of the deep VSA elements: 97.1 m, 102.1 m, 107.1 m and 112.1 m.

acoustic transect was approximately aligned with an isobath. For acoustic purpose, the environment is characterized by a slightly downward refracting sound speed profile in the water column (not shown, [8]), and the bottom is described by a

param. m_i (phys. unit)	"true" value	coeff. θ_i	lower bound	upper bound	dmmin_i $\times 10^{-5}$
Sediment layer sound speed					
c_l (m/s)	1470	100	1460	1500	1
Sediment layer density					
ρ_l (g/cm^3)	1.5	0.15	1.3	1.7	5
Sediment layer attenuation					
α_l (dB/λ)	0.03	0.15	0	0.5	5
Semi$-\infty$ bottom sound speed					
c_b (m/s)	1530	100	1500	1600	1
Semi$-\infty$ bottom density					
ρ_b (g/cm^3)	1.8	0.2	1.7	2.5	5
Semi$-\infty$ bottom attenuation					
α_b (dB/λ)	0.15	0.15	0	0.5	5

Table 1: Geoacoustic parameters of the Yellow Shark [14] reference environment and parameter settings for the minimization of the cost function (12).

layer of soft sediment (clay) with a compression wave speed smaller than the bottom water sound speed, overlying a halfspace of more consolidated sediment (silty clay) with a thin grainstone at the interface. The geoacoustic parameters of that environment are listed in Tab. 1 together with their reference "true" value [22].

This environment and measurement configuration constitute a realistic test case to investigate numerically the usefulness of vector (particle velocity or intensity flux) observations with respect to pressure observations alone. The test case is particularly interesting because results have been obtained that demonstrate the effectiveness of the sparse and compact array of hydrophones (OAA) for geoacoustic inversion purpose. The main question is how much can we expect by replacing the OAA with a VSA of the same length and with the same number of elements as the OAA. Here, two source-receiver geometries are considered: The first one is with the VSA covering the same depths as the OAA deployed for run #2 (shallow VSA) and the second one is with the VSA deployed just above the seafloor (deep VSA). (A deep OAA was also used during MREA/BP07 experiment but the data have not yet been processed.) The respective VSA element depths are given in Fig. 1.

In the actual run a signal sequence was repeatedly transmitted every minute consisting of a multitone signal with 1/12th-octave frequencies in the band 0.2–1.6 kHz, and two chirp signals covering the lower and higher half parts of the band [21]. Geoacoustic inversion results have been obtained with the three types of signals [8, 9, 23]. Here, a multitone signal with seven third-octave frequencies is considered: $\{200 \;\; 250 \;\; 315 \;\; 400 \;\; 500 \;\; 630 \;\; 800\}$ Hz. Figure 2 shows the pressure and vertical particle velocity fields at the frequency of 400 Hz, and the same components vs frequency and depth at the range of 1161 m, as calculated by the numerical WAPE model G for the geometry of Fig. 1 and "true" geoacoustic parameters of Tab. 1.

For the numerical study, the kth signal component received

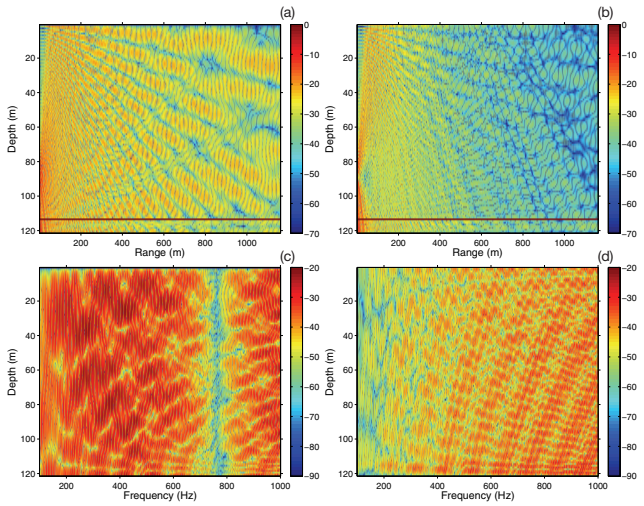

Figure 2: Real part of (a) acoustic pressure field p and (b) vertical component of the acoustic particle velocity field v_z at the frequency of 400 Hz. Real part of (c) acoustic pressure p and (d) vertical component of the acoustic particle velocity v_z vs frequency and depth at the range of 1161 m.

on the jth VSA elements, $s_{j,k}(t)$ ($j = 1, 2, 3, k = 1, \ldots, N$), is actually synthesized as

$$s_{k,j}(t) = F(d_{k,j}, t) + e_{k,j}(t), \tag{15}$$

where $d_{k,j}$ is the jth element of $\mathbf{d}_k = G_k(\mathbf{m})$, $\mathbf{m}$ is the set of true parameters, F is a function that transforms complex-valued components $\mathbf{d}_k$ into respective time series and $e_{k,j}(t)$ is a white noise with a standard deviation ν_k.

A reference variance ν_1^2 is first computed for the pressure component $e_1(t)$ as

$$\nu_1^2 = a^2 \sum_{j=1}^{N} \sum_{l=1}^{N_s} \frac{s_{1,j}^2(t_l)}{N\, N_s} \tag{16}$$

where a^2 is a coefficient that represents a fraction of the array signal average power, $s_{1,j}$ is the jth (pressure) signal ($j = 1, \ldots, N$) and N_s is the number of observation samples.

The autospectrum of pressure is related to the three particle velocity component autospectra: $S_p = (\rho_0 c_0) \sum_{j=1}^{3} S_{v_j}$. The variances ν_2^2 of $e_2(t)$ and ν_3^2 of $e_3(t)$ for the particle velocity components are computed from ν_1^2 as

$$\nu_{(2,3)}^2 = \frac{\nu_1^2}{3(\rho_0 c_0)^2} 10^{-\delta_{(2,3)}/10}, \tag{17}$$

where $\delta_{(2,3)}$ is the power level difference expressed in dB between the pressure and the respective particle velocity components, $c_0 = 1500$ m/s and $\rho_0 = 1$ g/cm^3. The difference depends on the noise model taking values of e.g., for spherically isotropic noise $\delta = 0$ dB for both components and for distant ship noise typically $\delta = 15$ dB–30 dB for the vertical component [24]. For the kth component of $\mathbf{y}_{k,0}$ and ith frequency the cross-spectral density matrix in "phone space" $\mathbf{R}_k^i$ in (12) is estimated from the corresponding array time series according to (5) and (6) of [14].

6 Ensemble adjoint inversion results

Although the proposed inversion scheme allows for any combination of the four VSA components the present focus is on comparing the relative performance of pressure and vertical particle velocity taken separately. The control vector $\mathbf{m}$ is composed of six geoacoustic parameters of the layered bottom as listed in Tab. 1. For the minimization, the corresponding true values, the coefficients θ and the resolution arguments dmmin_i are given in Tab. 1. The parameter epsg is taken equal to 10^{-9}.

6.1 Relative sensitivity of pressure and vertical particle velocity

Figures 3 and 4 show ensemble inversion results obtained from respectively the pressure and vertical particle velocity components of the shallow VSA with no measurement noise. The inversion process was repeated for 100 realizations of the initial conditions which were taken randomly within the predetermined search intervals between the lower and upper bounds indicated in Tab. 1. In view of the intervals it is emphasized that the resulting 6-dimensional search space is rather huge.

Figures 3(a) and 4(a) compare the cost function vs the iteration index for pressure (p) and vertical particle velocity (v_z) while Figs. 3(b) and 4(b) compare the corresponding convergence of the individual parameters. Figures 3(c) and 4(c) show, in the form of dots, all the solutions which were calculated during the adjoint-based forward-backward iterations. All 100 runs are aggregated in these graphics where each dot represents the value of a given parameter and the associated value of the cost function taken in the course of the minimization process.

In Fig. 3, pressure cost function shows a similar high sensitivity to both layer and halfspace compression wave speeds, and a good sensitivity to layer attenuation while a low sensitivity to the densities and bottom attenuation. This has been observed in previous work with global optimization using metaheuristics [8, 9, 23]. With regard to the comparison between p and v_z, the first observation is that for both p and v_z the adjoint-based optimization systematically converges to the correct, unbiased solutions independently of the random set of initial conditions [Figs. 3(b) and 4(b)]. The second observation is that the vertical particle velocity converges more rapidly than the pressure [Figs. 3(a) and 4(a)]. A third observation is that the densities and attenuations of both layer and subbottom converge faster for v_z than for p, as seen from one-to-one comparison of the ensemble convergence curves for the respective parameters [Figs. 3(b) and 4(b)]. It is emphasized that since the cost function minimization is directly and optimally controlled by the physics of acoustic propaga-

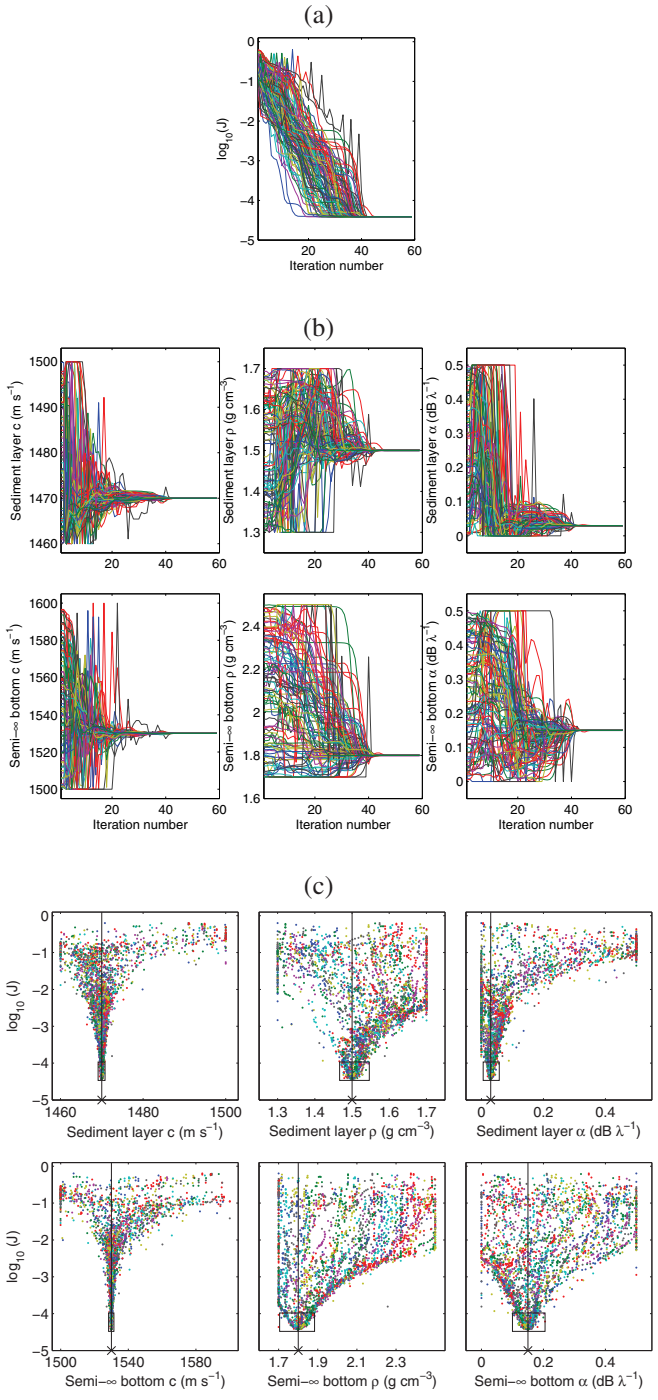

Figure 3: Ensemble adjoint inversion results from p measurements of the shallow VSA. (a) Convergence of the cost function $\log_{10}(J)$. (b) Convergence of the individual parameters c_l, ρ_l, α_l, c_b, ρ_b, α_b. (c) Parameter-cost function value pairs taken during the minimization process. The ensemble run is 100 realizations of the initial conditions.

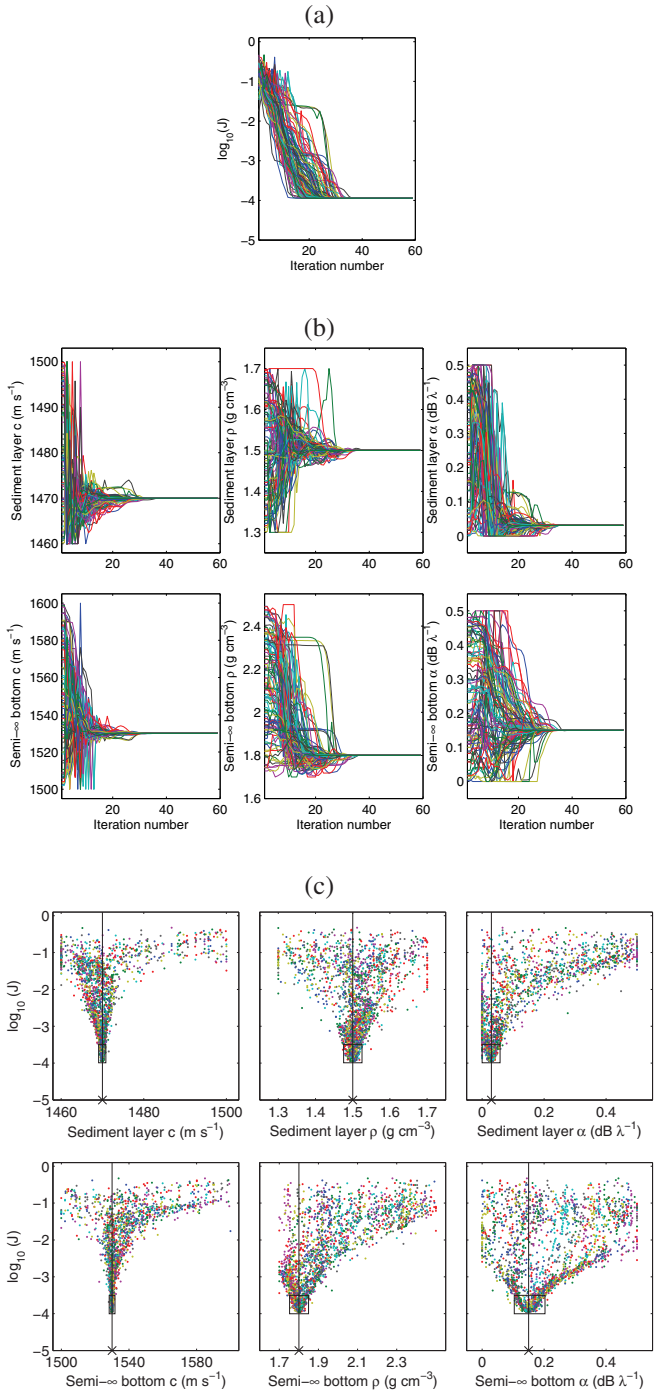

Figure 4: Ensemble adjoint inversion results from v_z measurements of the shallow VSA. (a) Convergence of the cost function $\log_{10}(J)$. (b) Convergence of the individual parameters c_l, ρ_l α_l, c_b, ρ_b, α_b. (c) Parameter-cost function value pairs taken during the minimization process. The ensemble run is 100 realizations of the initial conditions.

tion the convergence rates can be considered as good measure of sensitivity in contrast to global optimization using metaheuristics. It is also noted that for v_z the convergence of the sound speeds is more evenly balanced with the other parameters than for p. The higher sensitivity of vertical particle velocity v_z to densities and attenuations is confirmed by the representation of Figs. 3(c) and 4(c). Finally, it is noticeable that v_z-based solutions are less and more symmetrically scattered about the true solution than for p.

6.2 Dependence on observation depths

The same numerical experiment was carried out for an array placed just above the seafloor (deep VSA). Figures 5(a) and 5(b) compare the cost function vs the iteration index for p and v_z. From graphics similar to Figs. 3(c) and 4(c) the p observations are seen to have a sensitivity comparable to the v_z observations near the surface (not shown). The v_z observations do not further increase sensitivity with respect to pressure but provide more stable and somewhat faster convergence to the true solutions with no bias. For pressure, 5 out of 100 solutions are strongly biased.

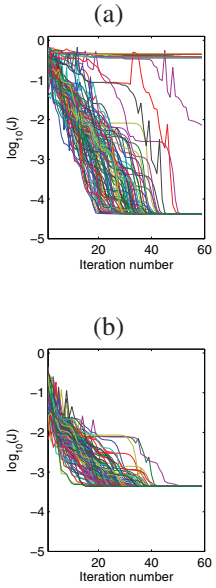

Figure 5: Convergence of the cost function $\log_{10}(J)$ for (a) p and (b) v_z data of the deep VSA.

6.3 Robustness to uncertainty

After evaluating the intrinsic sensitivity of the p and v_z observables to bottom geoacoustic parameters the robustness of these observables to uncertainty was examined. For this purpose a high level of Gaussian noise is added to the data with no inter-sensor correlation to represent, in a first approximation, both ambient noise [25] and modeling uncertainty. The internal (additive) vector sensor noise is not the major source of noise as compared to ambient noise. For pressure, the noise variance ν_1^2 is calculated from (16) with the coefficient a set equal to 0.3. This represents 30% of the signal average power on a reference array covering the water column, as estimated with $N = 23$ and $N_s = 6 \times 10^5$. For particle velocity, a spherically isotropic noise [$\delta = 0$ dB in (17)] is a worst case situation for the geoacoustic characterization of a shallow water environment using an active sound source. Here, it is assumed that there is no ship in the immediate proximity of the VSA and that the wind speed or sea state is low. Then, the vertical particle velocity is not perturbed by nearby ship selfnoise or sea surface noise. In addition the vertical component is relatively insensitive to noise from distant shipping in comparison to the horizontal components. For particle velocity, a power level difference δ in the range 15–30 dB is typical [24].

Figures 6 and 7 show the results for the shallow array p and v_z data perturbed by 100 realizations of the additive noises. For each noise realization the initial conditions are randomized. For both p and v_z, the convergence rates are similar to the respective noise-free results but the minimization yields a larger value of the cost function. For v_z the intermediate solutions for densities are more concentrated about the true solution than for p [Figs. 6(c) and 7(c)]. Furthermore the distributions of the attenuation parameters solutions are less affected by the noise perturbations for v_z than for p. For v_z the solutions have smaller bias and variance than for p, especially for the densities and bottom attenuation. In summary, the vertical particle velocity appears to be less sensitive to perturbation than pressure.

7 Conclusion

An ensemble adjoint approach has been proposed to study the relative sensitivity and robustness to uncertainty of acoustic pressure and vector data in inverting for shallow-water environmental properties, and in particular bottom geoacoustic properties. For a mimicked Yellow Shark environment and a sparse and compact array configuration of MREA/BP07 experiment, vertical particle velocity data are shown to enhance estimation of density and attenuation parameters of a soft layered bottom with respect to pressure, in particular for an array in the upper part of the water column. It should not be difficult to extend the proposed approach to any combination of pressure, particle velocity or intensity flux components, other cost functions and vector sensor array geometries to study other environments.

Acknowledgement

This work is supported by ONR 321OA and SHOM.

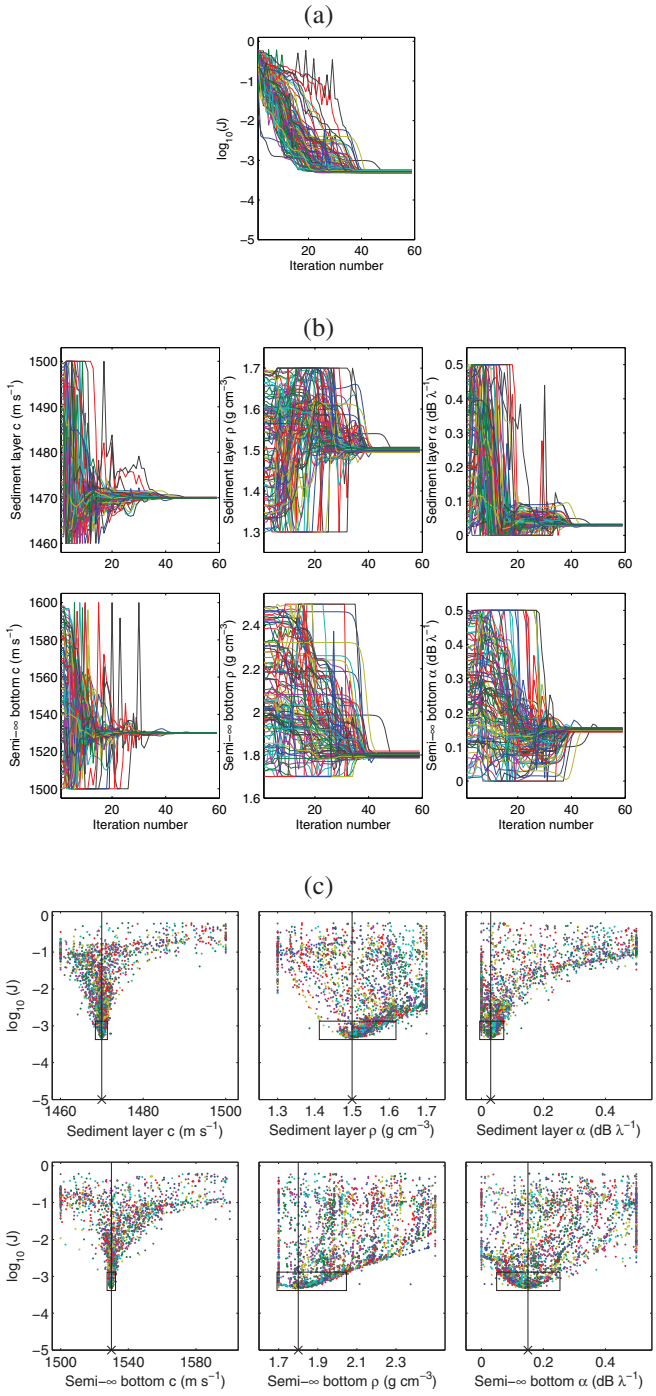

Figure 6: Ensemble adjoint inversion of noise perturbed p data of the shallow VSA. The ensemble run is 100 realizations of both additive noises and initial conditions.

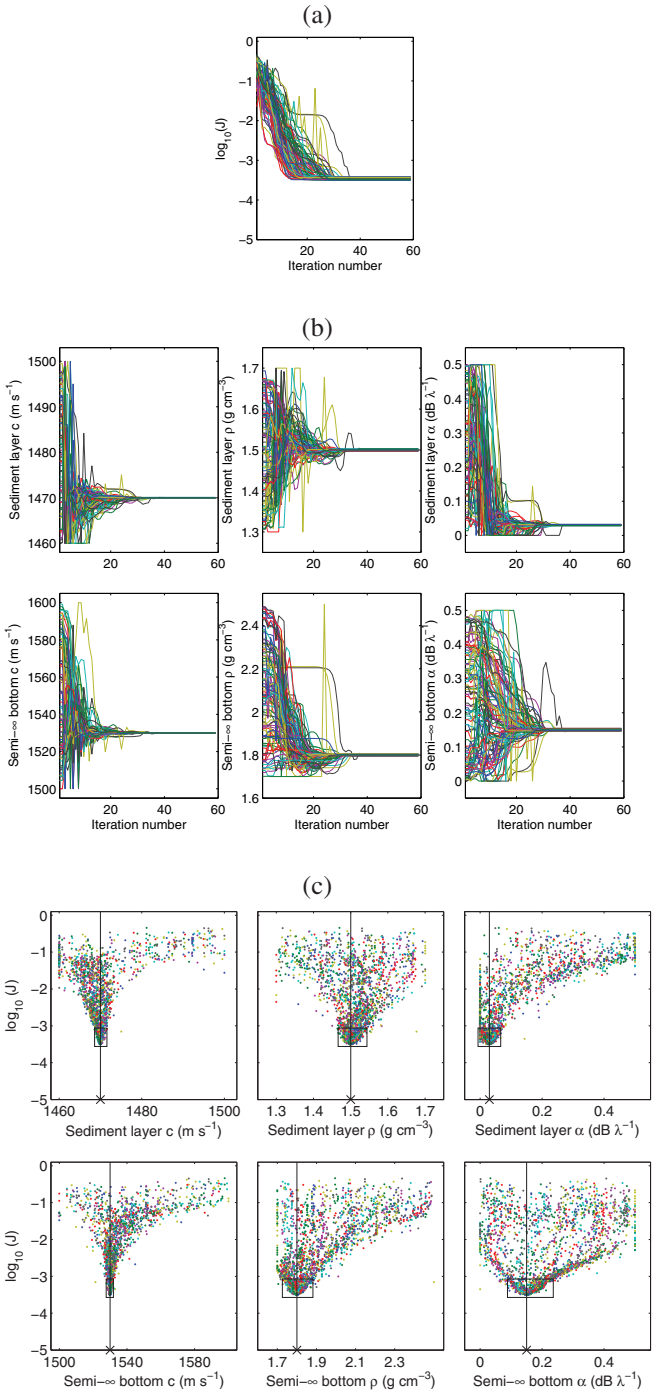

Figure 7: Ensemble adjoint inversion of noise perturbed v_z data of the shallow VSA. The ensemble run is 100 realizations of both additive noises and initial conditions.

References

[1] H. Peng and F. Li. Bottom attenuation inverted from a single vector sensor in shallow water. In *Proceedings of Acoustical Society of China Annual Meeting*, pages 143–144, October 2006.

[2] H. Peng and F. Li. Geoacoustic inversion based on vector hydrophone array. *Chin. Phys. Lett.*, 24(7):1977–1980, March 2007.

[3] M. Berrada, M. Meyer, J.-P. Hermand, M. Asch, and K.B. Smith. Efficient semi-automatic adjoint generation and its application for implementing acoustic particle velocity in geoacoustic inversion. In *8th International Conference on Theoretical and Computational*

Acoustics ICTCA, Heraklion, Crete, 2-6 July 2007.

[4] H. Peng and F. Li. Geoacoustic inversion from vector hydrophone array in shallow water. *Technical Acoustics*, 27(2):163–167, April 2008.

[5] P. Santos, P. Felisberto, O. Rodríguez, and S.M. Jesus. Geoacoustic matched-field inversion using a vector sensor array. In *Proceedings of the 2nd Int. Conf. on Underwater Acoustic Measurements*, June 2009.

[6] F. Li and R. Zhang. Geo-acoustic inversion with vector sensors in shallow water. *J. Acoust. Soc. Amer.*, 127(3):1856:2pUW2, March 2010.

[7] Q. Ren, S. Piao, and J.-P. Hermand. Investigation of the interference structure of broadband vector field in typical shallow environments. In *Proceedings of the European Ocean & Coastal Observation Conference (OCOSS)*, June 2010.

[8] J.-P. Hermand and J.-C. Le Gac. Subseafloor geoacoustic characterization in the kilohertz regime with a broadband source and a 4-element receiver array. In *Proceedings of OCEANS 2008 MTS/IEEE Quebec - Oceans, Poles and Climate: Technological Challenges, IEEE*, Quebec, September 2008.

[9] L. Maia, O. Carrière, C. Parente, and J.-P. Hermand. Acoustic inversion with a frequency-domain version of the model-based matched filter processing. In *Proceedings of the tenth European Conference on Underwater Acoustics*, July 2010.

[10] J.F. Claerbout. *Fundamentals of Geophysical Data Processing with applications to petroleum prospecting*. Blackwell Scientific Publications, 1976.

[11] D. Yevick and D.J. Thomson. Nonlocal boudary conditions for finite-difference parabolic equation solvers. *J. Acoust. Soc. Am.*, 106(1):143–150, July 1999.

[12] M. Meyer and J.-P. Hermand. Optimal nonlocal boudary control of the wide-angle parabolic equation for inversion of a waveguide acoustic field. *J. Acoust. Soc. Am.*, 117(5):2937–2948, May 2005.

[13] J.-P. Hermand, M. Meyer, M. Asch, and M. Berrada. Adjoint-based acoustic inversion for the physical characterization of a shallow water environment. *J. Acoust. Soc. Am.*, 119(6):3860–3871, March 2006.

[14] J.-P. Hermand and P. Gerstoft. Inversion of broad-band multitone acoustic data from the YELLOW SHARK summer experiments. *IEEE J. of Oceanic Eng.*, 21(4):324–346, October 1996.

[15] P. Gerstoft and C.F. Mecklenbrauker. Ocean acoustic inversion with estimation of a posteriori probability distributions. *J. Acoust. Soc. Am.*, 104(2), August 1998.

[16] L. Nardi, C. Sorror, F. Badran, and S. Thiria. YAO: A Software for Variational Data Assimilation Using Numerical Models. In O. Gervasi, D. Taniar, B. Murgante, A. Laganà, Y. Mun, and M.L. Gavrilova, editors, *LNCS 5593, Computational Science and Its Applications - ICCSA 2009*, pages 621–636. Springer-Verlag, 2009.

[17] F. Badran, M. Berrada, J. Brajard, M. Crépon, C. Sorror, S. Thiria, J.-P. Hermand, M. Meyer, L. Perichon, and M. Asch. Inversion of satellite ocean colour imagery and geoacoustic characterization of seabed properties: Variational data inversion using a semi-automatic adjoint approach. *Journal of Marine Systems*, 69:126–136, 2008.

[18] J.C. Gilbert and C. Lemarechal. The modules m1qn3 and n1qn3. Technical report, INRIA, March 1993.

[19] W.H Press, S.A Teukolsky, W.T. Vetterling, and B.P. Flannery. *Numerical Recipes in C*. Cambridge, 1995.

[20] H.W. Kuhn and A.W. Tucker. Nonlinear programming. In *Proceedings of 2nd Berkeley Symposium*, Berkeley, University of California, 1951.

[21] J.-C Le Gac and J.-P. Hermand. MREA/BP'07 cruise report. Technical Report NURC-CR-2007-04-1D1, NATO Undersea Research Centre, La Spezia, Italy, December 2007.

[22] J.-P. Hermand. Broad-band geoacoustic inversion in shallow water from waveguide impulse response measurements on a single hydrophone: Theory and experimental results. *IEEE J. of Oceanic Eng.*, 24(1):41–66, January 1999.

[23] L. Maia. *Inversão geoacústica e localização passiva de fontes em águas rasas*. Mestrado em engenharia oceânica, Instituto Alberto Luiz Coimbra de Pós-Graduação e Pesquisa de Engenharia (COPPE), Universidade Federal do Rio de Janeiro (UFRJ), Brazil, 2010.

[24] E.O. Ermolaeva, B.I. Goncharenko, and V.A. Gordienko. Vector-phase structure of the ocean noise field. In *Proceedings of the Pacific Rim Underwater Acoustics Conference 2007*, October 2007.

[25] M. Hawkes and A. Nehorai. Acoustic vector-sensor correlations in ambient noise. *IEEE J. of Oceanic Eng.*, 26(3):337–347, July 2001.